Mass Segregation in Globular Clusters

Fregeau, J.M.; Joshi, K.J.; Portegies Zwart, S.F.; Rassio, F.A.

DOI
10.1086/339576
Publication date
2002

Published in
Astrophysical Journal

The Astrophysical Journal, 570:171–183, 2002 May 1

MASS SEGREGATION IN GLOBULAR CLUSTERS

J. M. Fregeau,[1] K. J. Joshi,[2] S. F. Portegies Zwart,[3,4] and F. A. Rasio[5]
Received 2001 November 1; accepted 2002 January 10

ABSTRACT

We present the results of a new study of mass segregation in two-component star clusters, based on a large number of numerical N-body simulations using our recently developed dynamical Monte Carlo code. Specifically, we follow the dynamical evolution of clusters containing stars with individual masses m_1 as well as a tracer population of objects with individual masses m_2. We consider both light tracers ($\mu \equiv m_2/m_1 < 1$) and heavy tracers ($\mu > 1$) and a variety of King model initial conditions. In all of our simulations we use a realistically large number of stars for globular clusters, $N = 10^5$, but we ignore the effects of binaries and stellar evolution. For heavy tracers, which could represent stellar remnants such as neutron stars or black holes in a globular cluster, we characterize in a variety of ways the tendency for these objects to concentrate in or near the cluster core. In agreement with simple theoretical arguments, we find that the characteristic time for this mass segregation process varies as $1/\mu$. For models with very light tracers ($\mu \lesssim 10^{-2}$), which could represent free-floating planets or brown dwarfs, we find the expected depletion of light objects in the cluster core but also sometimes a significant *enhancement* in the halo. That is, for some initial conditions, the number density of light objects in the cluster halo increases over time, in spite of the higher overall evaporation rate of lighter objects through the tidal boundary. Using these results along with a simplified initial mass function, we estimate the optical depth to gravitational microlensing by planetary mass objects or brown dwarfs in typical globular clusters. For some initial conditions, the optical depth in the halo owing to very low mass objects could be much greater than that of luminous stars. If we apply our results to M22, using the recent null detection of Sahu, Anderson, & King, we find an upper limit of ~25% at the 63% confidence level for the current mass fraction of M22 in the form of very low mass objects.

Subject headings: celestial mechanics, stellar dynamics — globular clusters: general — methods: numerical — planetary systems — stars: low-mass, brown dwarfs

1. INTRODUCTION

Globular clusters are thought to contain objects with a very wide range of masses, although even the present-day mass function is rather poorly constrained by observations (see, e.g., Bedin et al. 2001). The initial mass function (IMF) is even less constrained, as it depends also on the details of the overall cluster dynamical evolution (Vesperini & Heggie 1997). Indeed, even for highly idealized systems of unevolving point masses, a wide mass spectrum, combined with the effects of two-body relaxation, leads to a variety of complex dynamical phenomena that are still poorly understood theoretically (Heggie et al. 1998). We will refer to these phenomena collectively here as "mass segregation," but note that they involve a number of different processes such as mass loss through the tidal boundary, energy equipartition and mass stratification, gravothermal contraction, and even in some cases gravothermal instabilities (see, e.g., Spitzer 1987).

The masses of directly observable stars today in globular clusters cover a relatively narrow range of ~1–2 $M_\odot$ (e.g., primordial binaries, blue stragglers, neutron stars; see, e.g., Bailyn 1995) down to ~0.1 $M_\odot$ at the faint end of the main sequence (e.g., Marconi et al. 1998). Much more massive stars were certainly present earlier in the dynamical evolution of these clusters, including more massive main-sequence stars and binaries, as well as primordial ~10 $M_\odot$ black holes (Portegies Zwart & McMillan 2000). Much lower mass objects such as brown dwarfs or planets may also have formed in large numbers within the cluster initially, and as we will show in this paper, significant numbers could also have been retained to the present.

Some lower mass objects ~10^{-2} to 10^{-3} $M_\odot$ have been detected in globular clusters as companions to millisecond radio pulsars (D'Amico et al. 2001; Ford et al. 2000; Freire et al. 2001). Gilliland et al. (2000) used the *Hubble Space Telescope* (*HST*) to search for transits by giant planets in short-period orbits ("hot Jupiters") around main-sequence stars in the central region of 47 Tuc. They reported a negative result and concluded that the planet frequency in 47 Tuc must be at least an order of magnitude below that for the solar neighborhood. However, in the high-density central region of this cluster, where the search was conducted, planetary systems are likely to be disrupted by encounters with other stars and binaries (Davies & Sigurdsson 2001), and the frequency of "free-floating" planets is not constrained by these observations. In contrast, gravitational microlensing can be used to try to detect such free-floating planets (Paczyński 1994). Analysis of microlensing events toward the Galactic bulge suggests the presence of a substantial amount of lower mass objects in globular clusters (Jetzer, Strässle, & Wandeler 1998). More recently, in a pioneering study, Sahu et al. (2001) monitored about 83,000 Galactic bulge stars for microlensing by objects in the globular cluster M22. They reported one clear microlensing

[1] Department of Physics, Massachusetts Institute of Technology, 77 Massachusetts Avenue, Cambridge, MA 02139; fregeau@mit.edu.
[2] Present address: 75 Peterborough Street, Number 313, Boston, MA 02215; kjoshi@alum.mit.edu.
[3] Astronomical Institute "Anton Pannekoek," University of Amsterdam, Netherlands; spz@space.mit.edu.
[4] Hubble Fellow.
[5] Department of Physics and Astronomy, Northwestern University, 2145 Sheridan Road, Evanston, IL 60208; rasio@northwestern.edu.

event associated with an object of about 0.1 $M_\odot$ and six events unresolved in time that were very tentatively associated with planetary mass objects in the cluster

Observational evidence for mass segregation has been found in a number of globular clusters. In some cases, direct evidence comes from the measurement of a more centrally concentrated density profile for some heavier stellar population, such as blue stragglers or radio pulsars (Côté, Richer, & Fahlman 1991; Layden et al. 1999; Rasio 2000). More often, the evidence comes from an apparent decrease in the slope of the (continuous) mass function toward the cluster core. This can either be estimated from the observed luminosity function at different radii (Howell et al. 2001; Sosin 1997) or inferred from color gradients (Howell, Guhathakurta, & Tan 2000). Note that in contrast to younger star clusters, where the present-day mass segregation may still reflect initial conditions (Figer et al. 1999; but see Portegies Zwart et al. 2002), any mass segregation observed in the central regions of globular clusters must be a result of dynamical evolution, since the relaxation time in those regions is typically much shorter than globular cluster ages (by a factor of ~ 10–10^3).

Our theoretical understanding of the dynamical evolution of dense star clusters containing a wide mass spectrum is far from complete, even in the highly idealized limit of unevolving point masses. Direct N-body simulations are very computationally intensive and have therefore been limited to systems with unrealistically low $N \sim 10^3$–10^4 and rather narrow mass spectra (de la Fuente Marcos 1996; Giersz & Heggie 1997; Takahashi & Portegies Zwart 2000). Since realistic IMFs are thought to increase (perhaps steeply) toward smaller masses, a lower mass cut-off (usually ~ 0.1–0.5 $M_\odot$) is introduced to avoid ending up with very few heavier objects and a large numerical noise in the simulation (since these heavier objects often dominate the overall dynamics).

Instead, in this paper, we use Hénon's Monte Carlo method to compute the dynamical evolution of clusters containing a more realistic number of stars ($N = 10^5$). Our Monte Carlo code, as well as a number of test calculations and comparisons with direct N-body integrations, have been described in detail in Joshi, Rasio, & Portegies Zwart (2000) and Joshi, Nave, & Rasio (2001). As a first step, we consider in this paper the simplest *two-component clusters*, in which only two types of objects, of mass m_1 and $m_2 \neq m_1$, are present. In addition, we assume that most objects in the cluster are of mass m_1, while the objects of mass m_2 form a *tracer population*; i.e., the total component mass ratio $M_2/M_1 \ll 1$. In general, the gravothermal evolution of a two-component cluster can be either stable or unstable, depending on the two ratios m_2/m_1 and M_2/M_1 (Spitzer 1969). In the stable case, the two components remain thermally coupled, and the cluster evolves dynamically toward energy equipartition between the two species. In the unstable case, energy equipartition is impossible, and the heavier species decouples thermally from the rest of the cluster, evolving separately toward core collapse and interacting with the lighter component through the mean gravitational field only. In a previous paper (Watters, Joshi, & Rasio 2000) we studied systematically the development of this instability (sometimes called the Spitzer "mass stratification" instability) in two-component systems, and we determined the location of the stability boundary in the parameter space of m_2/m_1 and M_2/M_1. Instead, in this paper, complementary to our previous study, we concentrate on the stable systems with $M_2/M_1 \ll 1$, and we study systematically the effects of their dynamical evolution toward energy equipartition. In particular, we seek to characterize quantitatively the tendency for heavier objects to develop radial density profiles that are more centrally concentrated, as well as the tendency for lighter objects to concentrate away from the central regions and to be preferentially evaporated in the Galactic tidal field.

Our paper is organized as follows. In § 2 we present an overview of our numerical approach, and we describe our initial conditions. In § 3 we present our results for light tracers (with $m_2 < m_1$), and we discuss their implications for microlensing by low-mass objects in globular clusters. In § 4 we present our results for heavy tracers (with $m_2 > m_1$), and we compare them to simple analytical estimates. Our conclusions and summary are presented in § 5.

2. OVERVIEW OF NUMERICAL METHOD

We study exclusively two-component clusters composed of point masses, ignoring the effects of binaries and stellar evolution. To evolve the clusters, we use our recently developed two-dimensional Monte Carlo code (Joshi, Rasio, & Portegies Zwart 2000), which is based on Hénon's Monte Carlo algorithm for solving the Fokker-Planck equation (Hénon 1971). Our code has shown close agreement with direct N-body and Fokker-Planck calculations of one-component clusters (Joshi, Rasio, & Portegies Zwart 2000), as well as calculations incorporating mass spectra and tidal mass loss (Joshi, Nave, & Rasio 2001). Furthermore, we have demonstrated reasonable agreement with the results of many different codes from Heggie's "collaborative experiment" (Heggie et al. 1998; see especially Rasio, Fregeau, & Joshi 2001, Fig. 2).

For the initial conditions, we use the King model (a lowered Maxwellian), given by the distribution function

$$f \begin{cases} \kappa\left(e^{\mathscr{E}/\sigma^2} - 1\right) & \text{for } \mathscr{E} > 0 \\ 0 & \text{for } \mathscr{E} \leq 0 \end{cases}, \tag{1}$$

where $\mathscr{E} \equiv \Psi - \frac{1}{2}v^2$ is the (negative) energy of each star relative to the potential at the tidal radius r_t, $\Psi \equiv -\Phi + \Phi(r_t)$ is the relative gravitational potential, and κ is a normalization constant. The quantity σ is a parameter and should not be confused with the actual velocity dispersion $(\langle v^2 \rangle)^{1/2}$. (See, e.g., Binney & Tremaine 1987 or Spitzer 1987.) For light tracers we enforce the tidal boundary induced by the Galaxy using a simple spherical Roche approximation (Joshi et al. 2001), while for heavy tracers (which tend to concentrate near the cluster center and hardly ever get ejected) we treat the clusters as isolated.

To effect a two-component distribution, we first create a single-component distribution of stars of mass m_1 according to equation (1) and then randomly replace a fraction of these background stars with tracers of mass m_2 so that the initial density profile of the tracers is the same as that of the background. Although this creates clusters that are initially slightly out of virial equilibrium, we find that they settle into virial equilibrium within a few crossing times (a few time steps). We have verified this independently using direct N-body integrations (see below), which relax to virial equilibrium within a few crossing times.

TABLE 1
MAIN RESULTS FOR LIGHT TRACERS

W_0	μ	N_t	N_b	$\frac{t_{cc}}{t_{rh}}$	$\frac{\tau_{1.5}(r_c)}{t_{rh}}$	$\frac{\tau_{10}(r_c)}{t_{rh}}$	$\frac{\tau_{1.5}(r_h)}{t_{rh}}$	$\frac{\tau_{10}(r_h)}{t_{rh}}$	$\frac{N_t(t_{cc})}{N_t(0)}$	$\frac{N_b(t_{cc})}{N_b(0)}$	$\frac{r_{ht}(t_{cc})}{r_{hb}(t_{cc})}$
1.....	0.001	1000	99,000	9.7	1.54	9.25	1.83	8.44	0.039	0.32	5.6
	0.001	15000	85,000	8.5	1.67	8.40	1.41	7.63	0.044	0.32	5.5
	0.004	1000	99,000	9.7	1.92	8.90	2.05	8.48	0.040	0.33	4.4
	0.01	1000	99,000	9.4	1.70	...	1.71	8.64	0.051	0.33	4.1
	0.04	1000	99,000	9.6	1.65	8.99	1.73	8.64	0.048	0.32	4.6
	0.1	1000	99,000	9.6	2.45	...	2.41	...	0.055	0.33	3.6
	0.2	1000	99,000	9.6	2.64	...	2.22	9.35	0.055	0.32	3.2
	0.4	1000	99,000	9.6	6.80	...	4.49	...	0.093	0.33	2.7
3.....	0.001	1000	99,000	11.7	0.90	11.63	1.44	10.45	0.076	0.46	2.9
	0.001	15000	85,000	10.1	0.87	...	0.97	8.70	0.086	0.46	3.2
	0.004	1000	99,000	11.6	1.05	11.13	1.41	10.57	0.079	0.46	2.9
	0.01	1000	99,000	11.7	1.08	10.63	1.65	10.13	0.068	0.46	3.2
	0.01	15000	85,000	10.0	1.13	...	1.03	8.90	0.088	0.46	3.0
	0.04	1000	99,000	11.6	1.46	...	1.55	10.93	0.10	0.46	3.1
	0.042	15000	85,000	10.2	1.09	...	1.13	9.37	0.094	0.46	3.0
	0.1	1000	99,000	11.7	1.05	...	1.74	...	0.11	0.46	2.8
	0.2	1000	99,000	11.7	1.99	...	2.35	11.65	0.11	0.46	2.5
	0.4	1000	99,000	11.7	10.61	...	5.61	...	0.16	0.47	2.2
5.....	0.001	1000	99,000	13.3	0.43	11.4	1.05	11.5	0.26	0.64	2.8
	0.001	15000	85,000	11.1	0.38	10.9	0.79	9.54	0.27	0.65	2.8
	0.1	1000	99,000	12.9	1.43	...	1.52	12.78	0.30	0.65	2.5
7.....	0.001	1000	99,000	8.7	0.57	8.31	0.87	7.22	0.68	0.87	2.3
	0.001	15000	85,000	7.6	0.21	2.30	0.70	7.25	0.68	0.87	2.2
	0.004	1000	99,000	9.0	0.67	7.24	1.07	8.20	0.67	0.86	2.3
	0.01	1000	99,000	8.9	0.50	6.90	1.00	8.77	0.68	0.87	2.1
	0.04	1000	99,000	9.0	0.54	6.20	1.08	...	0.68	0.87	2.2
	0.1	1000	99,000	8.9	0.54	8.44	1.17	...	0.70	0.87	2.0
	0.2	1000	99,000	8.9	0.70	...	1.28	...	0.73	0.87	2.1
	0.4	1000	99,000	8.8	1.76	...	2.51	...	0.77	0.87	1.8
9.....	0.001	15000	85,000	1.1	0.019	0.165	0.62	...	0.97	0.98	1.4
	0.1	1000	99,000	1.5	0.095	0.875	1.02	...	0.97	0.98	1.4

NOTE.—N_t: number of trace stars; N_b: number of background stars; t_{cc}: core collapse time; $\tau_{1.5}(r)$: time it takes for the number of tracers within radius r to decrease by a factor of 1.5 and $\tau_{10}(r)$ by a factor of 10; r_{ht} and r_{hb}: half-mass radii of the tracers and background stars, respectively. Ellipses represent data that were not attained before core collapse.

For light tracers (with mass ratio $\mu \equiv m_2/m_1 < 1$), we consider a variety of King models for the initial conditions, with dimensionless central potentials $W_0 \equiv \Psi(0)/\sigma^2 = \{1, 3, 5, 7, 9\}$, a variety of mass ratios in the range $0.001 \leq \mu \leq 0.4$, and a tracer population of either $N_t = 1000$ or $N_t = 15,000$ out of 10^5 total stars. Table 1 gives the initial conditions for each model. In all cases, tracers make up no more than 0.5% of the mass of each cluster and, consequently, do not significantly affect the overall evolution of the cluster.

For heavy tracers, we consider King models with $W_0 = \{3, 7, 10\}$, a variety of mass ratios in the range $1.5 \leq \mu \leq 10$, and a tracer population in the range $100 \leq N_t \leq 1000$. With a mass ratio greater than 1, it is not always feasible to use such a small number of tracers that the cluster is less than a few percent tracers by mass since then statistical noise is too great. Instead, we choose a reasonable value for the number of tracers and, consequently, explore both systems that can reach energy equipartition and systems that evolve away from thermal equilibrium. A simple test to determine whether thermal equilibrium is possible for a two-component cluster is the Spitzer stability condition (Spitzer 1969),

$$S \equiv \left(\frac{M_2}{M_1}\right)\left(\frac{m_2}{m_1}\right)^{3/2} \lesssim 0.16\,, \qquad (2)$$

where M_1 and M_2 are the total masses of species 1 and 2, respectively. If S is less than about 0.16, the system is "Spitzer stable," and the two components will reach thermal equilibrium. If S exceeds this value, the system is said to be "Spitzer unstable," and equipartition is impossible. Watters, Joshi, & Rasio (2000) performed a more refined analysis using our dynamical Monte Carlo code to evolve a wide range of two-component clusters and arrived at the more accurate empirical stability criterion

$$\Lambda \equiv \left(\frac{M_2}{M_1}\right)\left(\frac{m_2}{m_1}\right)^{2.4} \lesssim 0.32\,. \qquad (3)$$

Table 2 gives these stability parameters, as well as the initial conditions, for each model considered.

Some calculations with $\mu < 1$ were repeated with direct N-body integrations. For these direct N-body calculations, we used the program KIRA within the StarLab software environment[6] (see Portegies Zwart et al. 2001) and used the special purpose GRAPE-4 and GRAPE-6 hardware (a single GRAPE-6 board; Makino et al. 1997) to accelerate the computation of gravitational forces between stars. Time integration of stellar orbits was accomplished using a fourth-order Hermite scheme (Makino & Aarseth 1992).

[6] See http://www.manybody.org.

TABLE 2
MAIN RESULTS FOR HEAVY TRACERS

W_0	μ	N_t	N_b	S	Λ	$\frac{t_{cc}}{t_{rh}}$	$\frac{\tau_0(r_h < r < r_t)}{t_r}$	$\frac{\tau_{1.5}(r_c)}{t_{rh}}$	$\frac{\tau_{10}(r_c)}{t_{rh}}$	$\frac{\tau_{1.5}(r_h)}{t_{rh}}$	$\frac{r_{ht}(t_{cc})}{r_{hb}(t_{cc})}$
3.....	1.5	1000	99,000	0.028	0.040	16.50	0.74	0.52	11.61	1.30	0.070
	3	1000	99,000	0.16	0.42	7.60	0.27	0.33	3.85	0.54	0.099
	6	100	99,900	0.088	0.44	8.30	0.19	0.25	1.34	0.39	0.095
	10	100	99,900	0.32	2.5	3.20	0.13	0.42	1.61	0.44	0.080
	10	1000	99,000	3.2	25.4	1.50	0.16	0.37	1.36	0.37	0.18
7.....	1.5	1000	99,000	0.028	0.040	8.80	0.54	0.31	5.16	3.91	0.23
	3	1000	99,000	0.16	0.42	3.10	0.22	0.053	0.81	0.84	0.098
	6	1000	99,000	0.89	4.5	0.50	0.13	0.054	0.37	0.39	0.54
	10	1000	99,000	3.2	25.4	0.31	0.09	0.032	0.25	0.27	0.60
10....	1.5	200	99,800	0.0055	0.0080	0.38	0.31	0.028	0.37	...	0.85
	1.5	1000	99,000	0.028	0.040	0.38	1.5	0.028	0.32	...	0.98
	3	200	99,800	0.031	0.084	0.19	0.17	0.0021	0.043	...	0.86
	3	1000	99,000	0.16	0.42	0.081	0.6	0.0021	0.042	...	0.98
	6	200	99,800	0.18	0.89	0.022	0.09	0.0014	0.012	...	0.92
	6	1000	99,000	0.89	4.5	0.013	0.4	0.0016	...	...	1.0
	10	100	99,900	0.32	2.5	0.021	0.04	0.00050	0.0055	...	0.91

NOTE.—N_t: number of trace stars; N_b: number of background stars; S and Λ: stability parameters; t_{cc}: core collapse time; τ_0 (in units of t_r): mass segregation timescale; $\tau_{1.5}(r)$: time it takes for the number of tracers within radius r to *increase* by a factor of 1.5 and $\tau_{10}(r)$ by a factor of 10; r_{ht} and r_{hb}: half-mass radii of the tracers and background stars, respectively. Note that for each simulation the number of stars lost from the cluster was 1% or less. Ellipses represent data that were not attained before core collapse.

KIRA also incorporates block time steps (McMillan 1986a, 1986b; Makino 1991) and a special treatment of close two-body and multiple encounters of arbitrary complexity. Given the high cost of the direct N-body integrations, we limited our selection of initial conditions to a few models with $\mu < 1$ and performed the calculations with $N = 6144$ stars; these calculations take on the order of 10 days each to complete on either the GRAPE-4 or a single GRAPE-6 board. (With our Monte Carlo code, each calculation takes $\sim$12 hr.)

Following the convention of most previous studies, we define dynamical units so that $G = M_0 = -4E_0 = 1$, where M_0 and E_0 are the initial total mass and total energy of the cluster (Hénon 1971). The units of length, L, and time, T, are then

$$L = GM_0^2(-4E_0)^{-1} \quad \text{and} \quad T = GM_0^{5/2}(-4E_0)^{-3/2} . \quad (4)$$

Application of the virial theorem shows that L is the virial radius of the cluster and T is on the order of the initial dynamical (crossing) time. In the code, we use as the unit of time the initial relaxation time, t_r, which is given by

$$t_r = \frac{N_0}{\ln N_0} T , \quad (5)$$

where N_0 is the initial total number of stars in the cluster. For a two-component cluster, it is possible to define similar relaxation times for each component separately. The relaxation time for component 1, t_{r1}, is given by

$$t_{r1} = \frac{N_1}{\ln N_1} T_1 , \quad (6)$$

where N_1 is the initial number of stars of component 1, and T_1 is the crossing time for component 1 given by equation (4), with M_0 and E_0 replaced by the initial total mass and energy of component 1, respectively. The relaxation time for component 2, t_{r2}, is given analogously, although the resulting expression is only applicable when the two species have decoupled (e.g., a collection of black holes undergoing the Spitzer mass stratification instability).

To facilitate comparison with previous studies, we report times in this paper in units of the initial half-mass relaxation time, t_{rh}, given by the standard expression (see, e.g., Spitzer 1987)

$$t_{rh} = 0.138 \frac{N_0^{1/2} r_h^{3/2}}{\bar{m}^{1/2} G^{1/2} \ln N_0} , \quad (7)$$

where r_h is the initial half-mass radius, and $\bar{m} = M_0/N_0$ is the average stellar mass.

Each calculation is terminated when the 0.35% Lagrangian radius of the heavier component falls below 0.001 (in our length units). The Lagrangian radii are then inspected graphically and the core collapse time, t_{cc}, determined by noting the time at which the innermost Lagrangian radii of the heavier component begin to dip appreciably. Core collapse times determined in this way are not sensitive to the precise criterion used but can have a large statistical uncertainty, particularly when the number of stars within the innermost Lagrangian radii is small.

3. LIGHT TRACERS

Intuition has it that globular clusters cannot contain extremely light stars, since equipartition of energy would imply a mean velocity for the light stars that far exceeds the escape velocity for the cluster (Taillet, Longaretti, & Salati 1995). Although proportionately more light tracers than background stars are lost during the evolution, we find that a significant fraction are retained in the halo. In some cases their number density there actually increases during the evolution.

3.1. *Numerical Results*

To ensure the validity of our Monte Carlo results, we first sought to compare integrations performed with the Monte

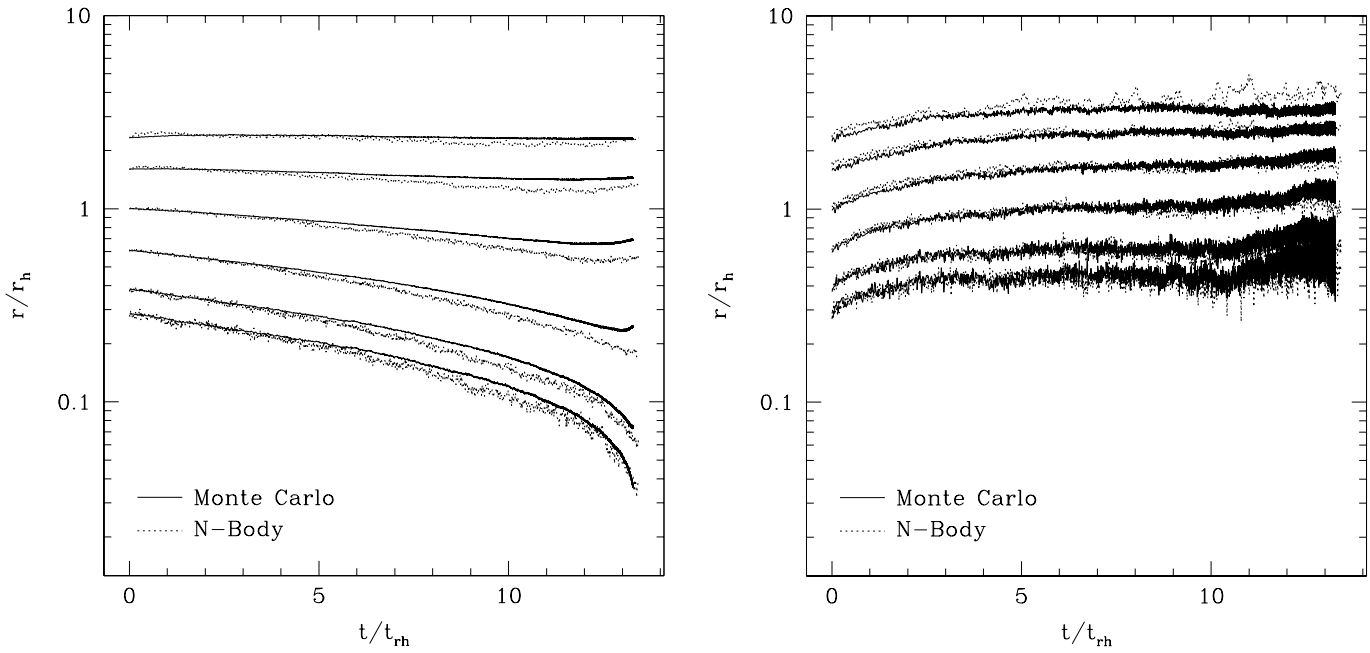

FIG. 1.—Comparison of Monte Carlo (*solid line*) and *N*-body (*dotted line*) data. Shown are the 5%, 10%, 25%, 50%, 75%, and 90% Lagrangian radii of background stars (*left*) and tracers (*right*) for a $W_0 = 5$ King initial model with a mass ratio $\mu = 0.001$, showing reasonable agreement between the two methods.

Carlo code with the results of direct *N*-body simulations. As a representative case, Figure 1 shows 5%, 10%, 25%, 50%, 75%, and 90% Lagrange radii (radii containing a constant mass fraction) for background stars (*left*) and tracers (*right*) for a $W_0 = 5$ King initial model with mass ratio $\mu = 0.001$. The agreement remains quite good at all times. The two methods agree remarkably in the most relevant result, that the light tracer stars "diffuse" into the outer halo, while the core, composed mainly of heavier "background" stars, contracts. This is consistent with the mass segregation found with previous *N*-body and Fokker-Planck studies (Spitzer 1987).

Figure 2*a* displays the segregation more clearly, showing *only* the Monte Carlo results from Figure 1. Here background stars are represented by a solid line, light tracers by a dotted line. As one expects from simple energy equipartition arguments, the tracers gain energy from interactions and are pushed out of the core, as is seen in the mass segregation evident as early as $t \simeq 5t_{\rm rh}$. However, 25% of the tracer population is left to linger in the outer regions at the time of core collapse. (By contrast, 65% of the background stars remain in the cluster.) Instead of receiving large monolithic kicks from the heavy stars and being immediately ejected from the cluster, the light tracers slowly gain energy and are gradually pushed out into the halo, where there are so few heavy stars that the light tracers are unable to exchange energy and are left there to linger. Figure 2*b* is the same as Figure 2*a* but for a very centrally concentrated $W_0 = 9$ King initial model. Because this cluster is initially so close to core collapse, it does not have much time to evolve; yet by the time of core collapse over 90% of the tracers occupy the outer region of the cluster in which 75% of the background stars reside. This extreme segregation is witnessed even for a more moderate mass ratio of $\mu = 0.1$. Figure 2*c* shows the same as Figure 2*a*, but for a $W_0 = 5$, $\mu = 0.1$ model. Here by the time of core collapse, about 90% of the tracers occupy the outer region in which 50% of the tracers reside.

For a more detailed look at the radial profile of the light tracers relative to the background, Figure 3*a* shows the number of stars in each radial bin. The number in each bin is divided by the *initial* total number of stars in the cluster, N_0, so that the vertical axis represents the fraction of stars in each bin. This histogram, which is proportional to dN/dr, is *not* a number density plot but still gives a feel for the number density and was chosen because it most clearly displays phenomena at large radii. Shown is the same $W_0 = 5$, $\mu = 0.001$ model as in Figure 1, with background stars in the top plot and tracers in the bottom. The dotted line represents a time very near the start of the simulation, while the solid line represents a time midway through the simulation, at $t = 4.9t_{\rm rh}$. There is a clear increase in the density of background stars in the core during the evolution, while there is also a clear decrease for tracers. More importantly, there is a significant *enhancement* of tracers in the halo region. Similarly, Figure 3*b* shows the same results for a $W_0 = 7$, $\mu = 0.001$ model. In this case, the number density of tracers in the halo is very visibly greater at core collapse than at the start of the simulation, and by about 50% in some regions. Even for the more modest mass ratio of $\mu = 0.1$, a similar profile is obtained, as shown in Figure 3*c*. Although a bit noisier than the preceding since only 1000 tracers are used here, the same significant enhancement of tracers in the halo is evident.

Table 1 gives relevant initial conditions for all the light tracer systems considered here, as well as core collapse times, the fraction of each species left in the cluster at core collapse, and the ratio of half-mass radii for the two species at core collapse. We have also included a few astrophysically relevant timescales: $\tau_{1.5}(r_c)$, the time for the number of light stars within the initial core radius to decrease by a factor of 1.5; $\tau_{10}(r_c)$, the time for the number of light stars within the initial core radius to decrease by a factor of 10;

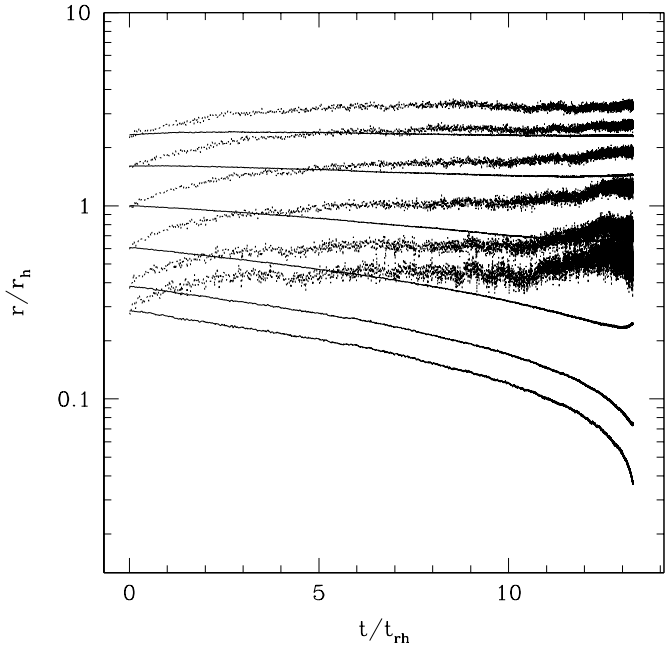

FIG. 2*a*

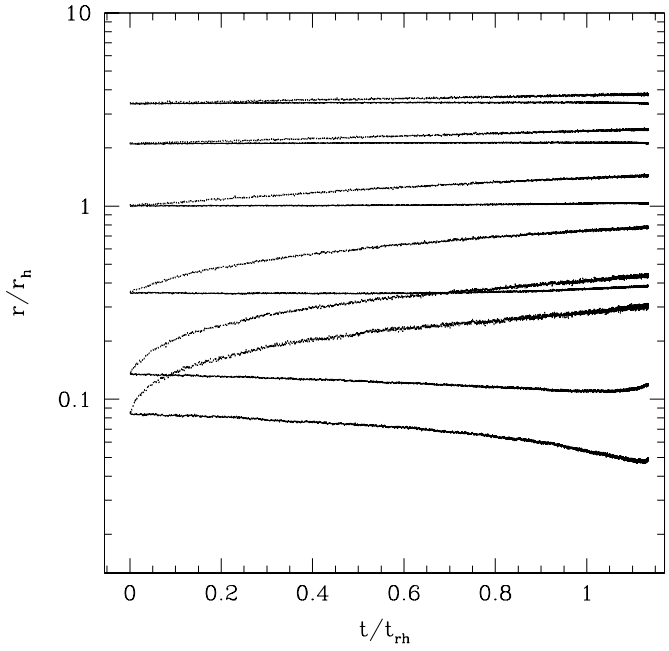

FIG. 2*b*

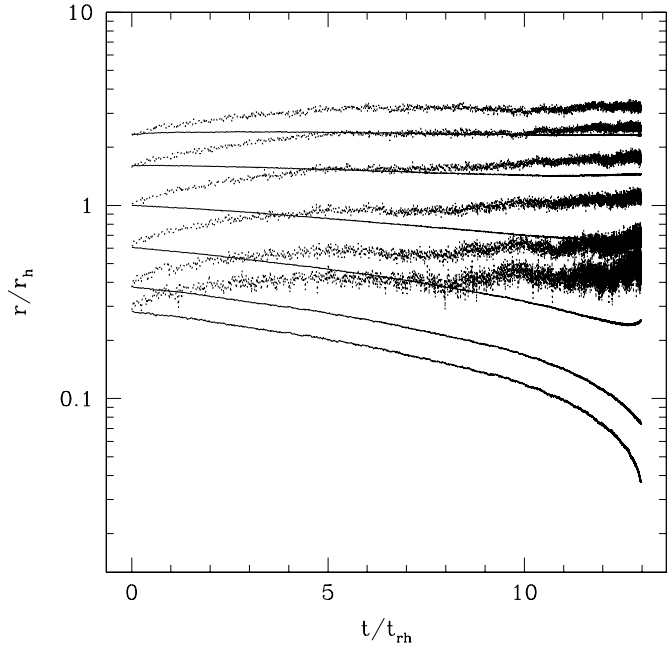

FIG. 2*c*

FIG. 2.—(*a*) Lagrangian radii of background stars (*solid line*) and tracers (*dotted line*) from Fig. 1, showing only the Monte Carlo results. Note the stark contrast between the two, illustrating the extreme mass segregation present even early in the simulation, at $t \sim 5\ t_{\rm rh}$. By core collapse, over 90% of the tracers occupy the outer region of the cluster in which 50% of the background stars reside. (*b*) Same as (*a*), but for a very centrally concentrated $W_0 = 9$ King initial model. Even though this cluster reaches core collapse very quickly (because it is initially almost core-collapsed), by that time over 90% of the tracers occupy the outer region of the cluster in which 75% of the background stars reside. (*c*) Same as (*a*), but for a mass ratio $\mu = 0.1$. Almost the same degree of mass segregation present for the extreme mass ratio of $\mu = 0.001$ is witnessed for this more reasonable value. Again, by core collapse, about 90% of the tracers occupy the outer region of the cluster in which 50% of the background stars reside.

$\tau_{1.5}(r_h)$, the time for the number of light stars within the initial half-mass radius to decrease by a factor of 1.5; and $\tau_{10}(r_h)$, the time for the number of light stars within the initial half-mass radius to decrease by a factor of 10. Figure 4 shows a representative determination of these timescales. Smooth curves were fitted to the data using GNUPLOT's "acsplines" (approximation cubic splines) routine. The timescales show a clear trend, increasing as the mass ratio approaches unity, consistent with energy equipartition arguments. A closer look reveals a critical mass ratio, around 0.3, below which the timescales τ_{10}, and especially $\tau_{1.5}$, are roughly constant; the light stars are so light that they are immediately ejected from the inner regions of the cluster on a timescale that is independent of mass ratio. A

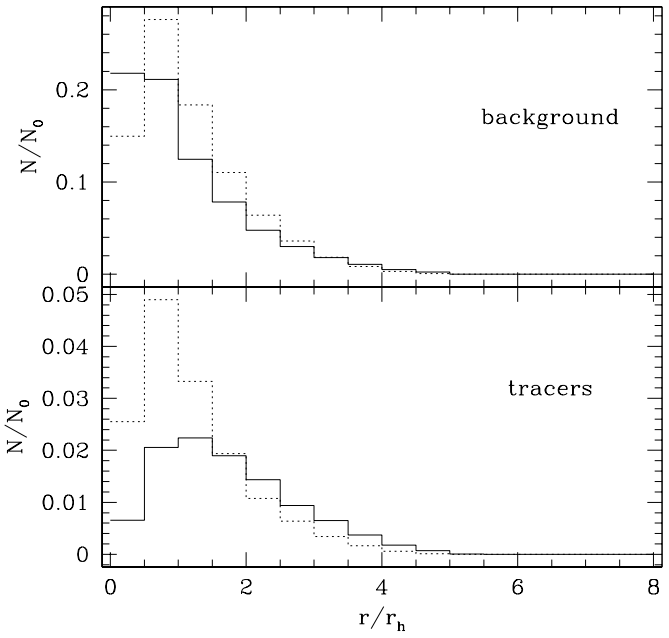

FIG. 3*a*

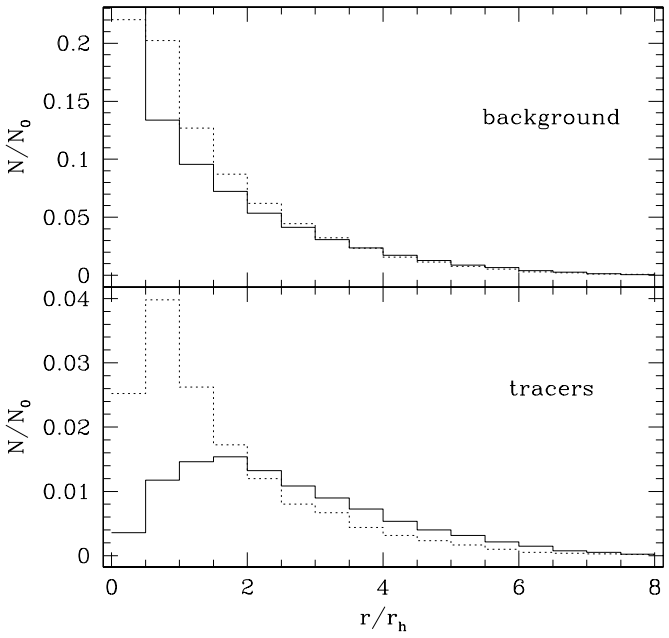

FIG. 3*b*

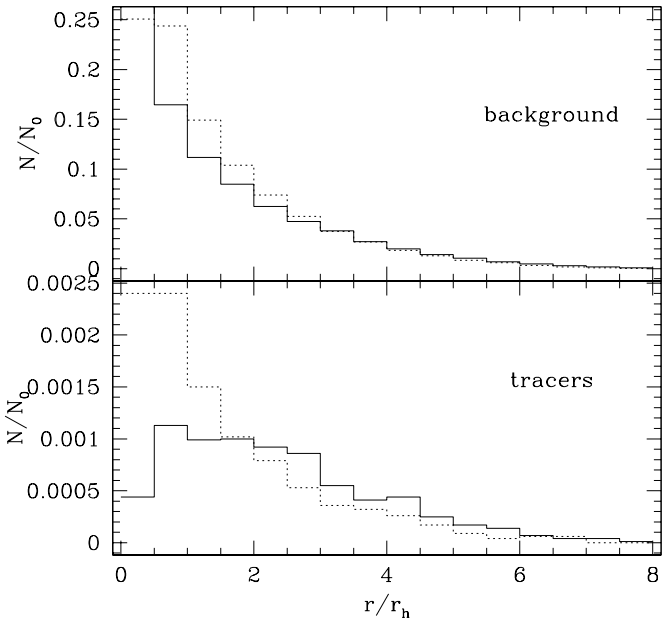

FIG. 3*c*

FIG. 3.—(*a*) Number histogram of stars vs. radius for a $W_0 = 5$ King initial model with a mass ratio $\mu = 0.001$, showing background stars in the top plot and tracers in the bottom. The dotted line represents a time very near the start of the simulation, while the solid line represents a time midway through the simulation, at $t = 4.9\ t_{\rm rh}$. While this is *not* a number density plot, it gives a feel for the radial profile of the two species. (*b*) Same as (*a*), but for a $W_0 = 7$ King initial model. Here the solid line represents a time near collapse, $t = 7.3\ t_{\rm rh}$. In this case, the number density of tracers in the halo is very visibly greater at core collapse than at the start of the simulation, and by about 50% in some regions. (*c*) Same as (*a*), but for a $W_0 = 7$ King initial model with a mass ratio $\mu = 0.1$. Again, the solid line represents a time near core collapse, $t = 7.2\ t_{\rm rh}$. Although the curve is a bit noisy, there is clearly an enhancement in the number density of tracers in the halo, even at this modest mass ratio.

simple derivation of this critical mass ratio, $\mu_{\rm crit}$, proceeds as follows. The escape speed from the center of the cluster is given by $v_e^2 = 2\Psi(0) = 2W_0\sigma^2$. In the core of the cluster, densities are very high, and it is expected that the two stellar species will attain thermal equilibrium: $\langle v_1^2\rangle_{\rm core} = \mu\langle v_2^2\rangle_{\rm core}$. Since the cluster is dominated by the heavy species (species 1), its velocity dispersion can be obtained directly from the distribution function (eq. [1]):

$$\langle v_1^2\rangle_{\rm core} \equiv \frac{\int_0^{\sqrt{2\Psi(0)}} v^2 dv f(0,v) v^2}{\int_0^{\sqrt{2\Psi(0)}} v^2 dv f(0,v)} \,. \tag{8}$$

This equation can be integrated numerically to give $\langle v_1^2\rangle_{\rm core}$

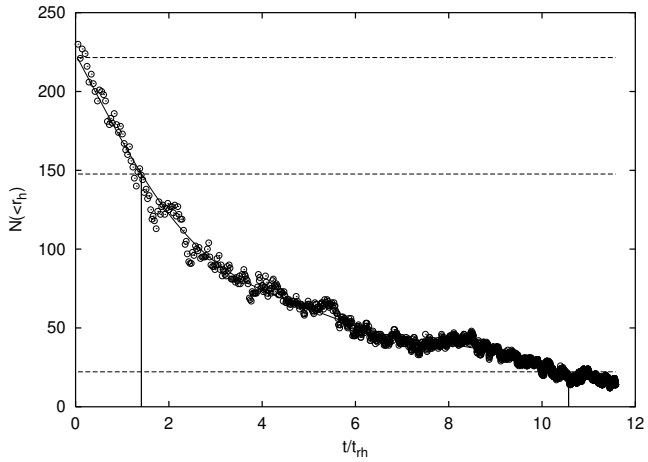

FIG. 4.—Representative determination of the mass segregation timescales $\tau_{1.5}(r_h)$ and $\tau_{10}(r_h)$ from Table 1 for the case $\mu = 0.004$, $W_0 = 3$. The top dashed line is the number of tracers initially within the half-mass radius, $N_0(r_h)$, the middle dashed line $N_0(r_h)/1.5$, and the bottom dashed line $N_0(r_h)/10$.

in units of σ^2: $\langle v_1^2 \rangle_{\rm core} \equiv \alpha\sigma^2$. Setting the velocity dispersion of the lighter species equal to the escape speed at the center yields a simple equation for the critical mass ratio,

$$\mu_{\rm crit} = \frac{\alpha}{2W_0} , \tag{9}$$

below which the light stars are almost immediately ejected from the core (within a core relaxation time) but not necessarily from the cluster. Table 3 gives α and $\mu_{\rm crit}$ for many values of W_0. Comparison with Table 1 shows that, indeed, below this mass ratio the light stars are ejected from the central regions of the cluster on a timescale that is independent of mass ratio; above this mass ratio, the segregation timescale increases dramatically.

TABLE 3
VELOCITY DISPERSION AND CRITICAL MASS RATIO

W_0	$\frac{\langle v_1^2 \rangle_{\rm core}}{\sigma^2}$	$\mu_{\rm crit}$
1.....	0.799	0.399
2.....	1.466	0.367
3.....	1.990	0.332
4.....	2.373	0.297
5.....	2.632	0.263
6.....	2.796	0.233
7.....	2.892	0.207
8.....	2.945	0.184
9.....	2.973	0.165
10.....	2.987	0.149
11.....	2.994	0.136
12.....	2.997	0.125

NOTE.—Velocity dispersion in the core in units of the velocity dispersion parameter σ, and critical mass ratio for immediate ejection from the core for many values of the dimensionless central potential W_0; see the discussion preceding eq. (9).

3.2. *Implications for Microlensing*

It is possible that globular clusters could contain copious amounts of nonluminous matter—often referred to as (baryonic) dark matter in this context (Heggie, Griest, & Hut 1993; Taillet, Longaretti, & Salati 1995; Heggie & Hut 1996). However, it is probable that the amount of dark matter is poorly constrained by observations of luminous stars. Consider a cluster with a continuous Salpeter IMF,

$$\frac{dN}{dM} \propto M^{-2.35} . \tag{10}$$

Since we want to study very light objects, let the IMF extend from 0.001 to 10 $M_\odot$ (even though such a mass function was never meant to apply below $\sim$0.1 $M_\odot$!). To place this problem in the context of two-component clusters, break up the IMF into two bins: a tracer bin extending from 0.001 to 0.1 $M_\odot$ corresponding to nonluminous objects and a background bin extending from 0.1 to 10 $M_\odot$ corresponding to main-sequence stars. (For simplicity, we will ignore stellar evolution and suppose that the heavy stars keep their mass for the lifetime of the cluster.) Integrating equation (10) over these two bins gives a mean tracer mass of 0.0031 $M_\odot$, a mean background mass of 0.31 $M_\odot$, and a ratio of the number of tracers to background of $N_t/N_b = 500$. Using the background stars as species 2 in equations (2) and (3), we find $S = 200$ and $\Lambda = 1.3 \times 10^4$; this simple model is well outside the Spitzer stability regime. The two species will decouple completely and evolve independently; observations of the luminous background stars will not betray the presence of the very light tracers.

Approximating the continuous mass spectrum by two bins is most likely unjustified, however, since in a continuous mass spectrum stars of mass M will certainly exchange energy with stars of mass $M + dM$. Thus, light stars will exchange energy with slightly heavier stars, which will exchange energy with slightly heavier stars, etc., providing an indirect means for light objects such as Jupiters to exchange energy with heavy objects such as main-sequence stars. Thus, thermal equilibrium among all species may not be forbidden in a realistic cluster, but the timescale over which it occurs is unclear.

Taillet, Longaretti, & Salati (1995) and Taillet, Salati, & Longaretti (1996) considered multicomponent King models and assumed that thermal equilibrium *did* occur among species. Using analytical methods, they found that the cluster surface brightness was nearly unaffected by the amount of nonluminous stars present, for a cluster with dark matter content ranging from 0% to 90% by mass. Therefore, observations of the luminous cluster stars would give no evidence of the dark matter in the cluster. (However, in the most extreme cases, the projected velocity dispersion profiles could be used to detect dark matter by observing the luminous component.)

Regardless of whether thermal equilibrium occurs in clusters, it is probable that dark matter would not be easily detectable by observing the luminous members of clusters. Dark matter could be directly detected, however, by its gravitational lensing effect on distant, luminous sources (Paczyński 1986, 1991, 1994). By convention, a microlensing event is said to occur when a background source lies, in projection, within the Einstein radius of a lens and is consequently amplified by a factor greater than 1.34 (Refsdal 1964; Vietri & Ostriker 1983). The optical depth, τ, is the

probability that such an event will occur and for low probability is given by

$$\tau = \frac{1}{\delta\omega}\int dVn(D_d)\pi\theta_{\rm E}^2 \,, \tag{11}$$

where $\delta\omega$ is the solid angle of sky considered, $dV = \delta\omega D_d^2 dD_d$ is the element of volume, n is the number density of lenses, D_d is the distance to the lens (deflector), and $\theta_{\rm E}$ is the angular Einstein radius of the lens. The Einstein radius is given by the usual expression

$$\theta_{\rm E}^2 = \frac{4GM}{c^2}\frac{D_s - D_d}{D_d D_s} \,, \tag{12}$$

where D_s is the distance to the source. Here we will be considering lensing of sources in the Galactic bulge, for example, by globular clusters along the line of sight to the bulge; therefore, typical values for D_d and D_s are $\sim$3 and $\sim$8 kpc, respectively. Since tidal radii of globular clusters are typically on the order of tens of parsecs, we can approximate D_d and D_s as constant over the range of integration to arrive at the simpler expression

$$\tau = \frac{4\pi G}{c^2}\Sigma(r)D_d\left(1 - \frac{D_d}{D_s}\right) \,, \tag{13}$$

where $\Sigma(r)$ is the surface density along the line of sight, and r is the distance perpendicular to the line of sight.

Figure 5*a* shows the optical depth owing to heavy stars (*solid line*) and light stars (*dotted line*) for a $W_0 = 3$ initial King model with 15,000 tracers of mass ratio $\mu = 0.01$. We have assigned the background stars a mass of 0.31 $M_\odot$ and multiplied the tracer number density by a factor $500 \times (85,000/15,000)$, consistent with the preceding discussion of approximating the Salpeter IMF by two mass bins. (This heuristic model therefore defines a thermally equilibrized two-component idealization of the continuous mass function.) We have also multiplied both optical depths by a factor of 5 so that the figure is normalized to a cluster that initially had 5×10^5 stars and a mass of 1.3×10^5 $M_\odot$. Generic values of $D_d = 3$ kpc and $D_s = 8$ kpc were used in the calculation, and this snapshot of the system was taken at $t = 9.5t_{\rm rh}$. Note not only the mass segregation, but also that at large radii the optical depth owing to the light stars is about an order of magnitude greater than that owing to the heavy stars. Significant numbers of nonluminous stars may linger in the outer regions of globular clusters.

3.3. *Dark Matter in M22*

Sahu et al. (2001) have carried out *HST* observations of the central regions of the globular cluster M22 (NGC 6656) and have detected at least one microlensing event. All the parameters needed to deduce the mass of the lens from the timescale of the lensing event are fairly well known so that a prediction of its mass can be made. Assuming distances of 8.2 kpc to the source (for a typical star in the Galactic bulge) and 2.6 kpc to M22, as well as a proper motion for M22 of 10.9 mas yr^{-1} (134.4 km s^{-1}), they determine the mass of the lens to be $0.13^{+0.03}_{-0.02}$ $M_\odot$. This result is exciting because it is the first such detection where the mass of the lens can be estimated. They also report a tentative detection of 6 sub-$M_{\rm J}$ objects in the core (an upper limit of $\sim$0.25 $M_{\rm J}$ for each) that has since proven spurious (Sahu, Anderson, & King 2002). Although the events are no longer associated with planets, we still present our theoretical analysis of the amount of dark matter in M22 as a useful exercise, illustrating how

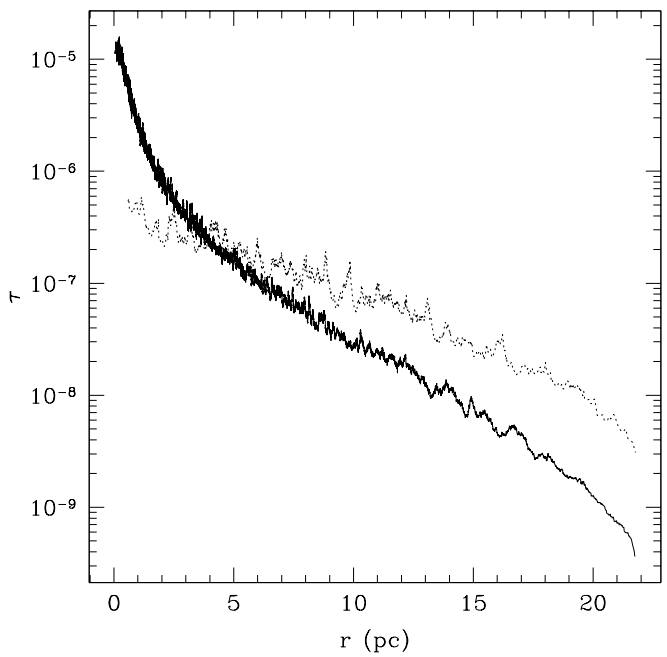

FIG. 5*a*

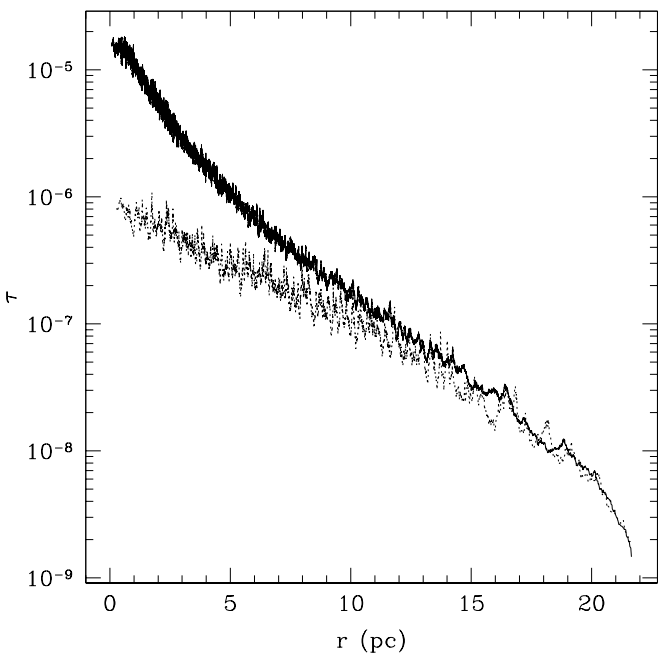

FIG. 5*b*

FIG. 5.—(*a*) Optical depth to microlensing owing to heavy stars (*solid line*) and light stars (*dotted line*) for a $W_0 = 3$ initial King model with 15,000 tracers of mass ratio $\mu = 0.01$. The number density of light stars has been amplified to emulate a continuous Salpeter IMF. This snapshot was taken near core collapse, at $t = 9.5$ $t_{\rm rh}$. Generic values of $D_d = 3$ kpc and $D_s = 8$ kpc were used in the calculation. (*b*) Optical depth to microlensing at present owing to luminous stars (*solid line*) and dark matter (*dotted line*) for the globular cluster M22.

future detections could be used to estimate the amount of dark matter in clusters.

It is a simple matter to calculate the optical depth owing to dark matter given these detections. Since the lenses are moving with respect to the source, the actual probability for microlensing is modified from equation (11) to

$$\text{Prob} \equiv \frac{N_e}{N_o} = \frac{1}{\delta\omega} \int dV n(D_d) 2\theta_{\rm E} \dot{\varphi} \Delta t \ , \qquad (14)$$

where N_e is the number of microlensing events observed, N_o is the number of observations, $\dot{\varphi}$ is the angular velocity of the lens, and Δt is the time duration of each observation. In terms of the optical depth, this is simply

$$\frac{N_e}{N_o} = \frac{2}{\pi} \tau \frac{\Delta t}{t_0} \ , \qquad (15)$$

where $t_0 \equiv \theta_{\rm E}/\dot{\varphi}$ is the characteristic timescale of a microlensing event. The optical depth is then

$$\tau = \frac{\pi}{2} \frac{N_e}{N_o} \frac{t_0}{\Delta t} \ . \qquad (16)$$

Sahu et al. (2001) monitored approximately 83,000 stars for a period of $\sim$105 days and found six candidate dark matter (below 0.1 $M_\odot$) microlensing events lasting at most 0.8 days each. Equation (16) then gives an optical depth owing to dark matter of 8.7×10^{-7}. Adopting the same simple prescription used before of approximating a continuous mass function by two mass bins, we can evolve a two-component cluster from a reasonable initial state until its profile resembles that of M22. We can then adjust the number of tracers so that the optical depth in the core owing to dark matter matches observations and, consequently, estimate what fraction of the cluster mass would have been in dark matter had the six tentative detections proven correct.

For our initial conditions we take a $W_0 = 3$ King model with 85,000 background stars of 0.38 $M_\odot$ and 15,000 tracers of 0.016 $M_\odot$ to emulate a Kroupa IMF—which we have extended well below the $0.1 M_\odot$ lower limit for which it was intended—from 0.001 to 10 $M_\odot$ split into two bins at 0.1 $M_\odot$ (Kroupa, Tout, & Gilmore 1993). The Kroupa IMF is more conservative than a Salpeter IMF in that it contains far fewer sub–stellar-mass objects. (The exact form of the IMF chosen is largely irrelevant, since in the end we scale the number of stars in each mass bin to match observations; however, it may affect the percentage of light stars lost from the cluster during evolution.) We then evolve the cluster until its profile matches that of M22, approximately a $W_0 = 6$ model (Harris 1996). We adjust the number of background stars so that the mass owing to luminous matter is $10^{5.57}$ $M_\odot$ (Mandushev, Spassova, & Staneva 1991) and adjust the number of tracer stars so that the optical depth owing to dark matter in the core is approximately 8.7×10^{-7}.

Figure 5*b* shows the optical depth owing to luminous stars (*solid line*) and dark matter (*dotted line*) using the prescription just given. Adopting the total cluster mass and dark matter optical depth quoted above, we find that the current mass of M22 would have been $\sim$20% dark matter by mass. If either the total cluster mass or optical depth are off by a factor of 2, this number could be as small as 12% or as high as 35%. If both are off by a factor of 2, then this number could be as small as 6% or as high as 52%. This range of values is consistent with the value quoted by Sahu et al. (2001) of $\sim$10% but implies a higher median. Using the median values, this analysis implies that M22 would have had an initial mass of 8.3×10^5 $M_\odot$, 35% of which was dark matter (this figure could be anywhere between 12% and 69%) and that it would have lost 2×10^5 $M_\odot$ of dark matter to the Galaxy. These ranges of values should be treated with caution, however, since our Monte Carlo code ignores the effects of binaries, mass loss owing to stellar evolution, and the effects of a nonspherical tidal field, all of which may affect the fraction of light tracers retained in a cluster. Furthermore, it is clear that in order to tighten constraints on the amount of dark matter, one must also refine estimates of the distances to the lens and the source.

3.4. *Upper Limit on Dark Matter in M22*

All six "planetary" events are no longer interpreted as being due to microlensing. More careful examination reveals that the apparent brightening observed in both of a pair of cosmic-ray split images was actually due to pointlike cosmic rays hitting close to the same star in both images (Sahu, Anderson, & King 2002). This null detection, while unfortunate, can be used to estimate an upper limit on the mass fraction of M22 in very low mass objects.

Adopting our simple prescription of approximating the continuous mass function by two bins, one containing luminous matter (objects heavier than 0.1 $M_\odot$), the other containing dark matter (objects lighter than 0.1 $M_\odot$), we assume that the dark matter in M22 is represented by a collection of objects with the average mass in that bin, 0.016 $M_\odot$. We then expect the number of dark matter lensing events in an observation to obey a Poisson distribution. Adopting a mean of one dark matter lensing event, using $t_0 \approx 6$ days for a 0.016 $M_\odot$ lens, and performing essentially the same analysis as in § 3.3, a null detection yields an upper limit on the current mass fraction of M22 in very low mass objects of $\sim$25% at the 63% confidence level. Adopting a mean of three events yields an upper limit of $\sim$50% at the 95% confidence level.

Although our simple calculation is physically motivated, it is necessarily crude, since a careful analysis should take into account the mass distribution of the dark matter. In addition, there is another effect to consider. The typical separation between exposures in the Sahu et al. (2001) observation is about 3 days. Thus, a microlensing event with characteristic width smaller than 3 days, corresponding to a lens mass of 0.004 $M_\odot$, has a nonzero probability of not being detected, biasing detections toward higher masses. Since the smallest mass we consider is 0.001 $M_\odot$, presumably this effect is small.

4. HEAVY TRACERS

4.1. *Analytic Results*

Spitzer (1969) pioneered the theoretical analysis of mass segregation in clusters. Considering a two-component cluster in which one component is more massive than the other, yet sparse enough to be considered a tracer population, he found that the timescale on which the heavier species contracts varies approximately as $1/\mu$. For completeness, we include a brief summary of the steps leading to this result.

For the generic case of energy transfer when E_2, the mean kinetic energy of the massive stars, is greater than the corre-

sponding energy E_1 for the lighter stars, the rate of energy loss of the massive stars is given by

$$\frac{dU_2}{dt} = \frac{(E_1 - E_2)}{t_{\rm eq}} , \tag{17}$$

where U_2 is the mean total energy of the heavier species. The equipartition time is approximately (Spitzer 1940, 1962)

$$t_{\rm eq} = \frac{\left(\langle v_1^2\rangle + \langle v_2^2\rangle\right)^{3/2}}{8(6\pi)^{1/2}\rho_{01} G^2 m_2 \ln N_1} , \tag{18}$$

where ρ_{01} is the central density of the lighter species, N_1 is the number of light stars in the cluster, and brackets denote an average over stars. When one expresses this timescale in units of $t_{\rm r1}$, the overall relaxation timescale of species 1, one obtains

$$\frac{t_{\rm eq}}{t_{\rm r1}} = \frac{3\pi^{1/2}}{16}\frac{m_1}{m_2}\left(1 + \frac{\langle v_2^2\rangle}{\langle v_1^2\rangle}\right)^{3/2} . \tag{19}$$

It follows that if the rms velocities of the two species are equal, as they are at the start of our simulations (they remain roughly equal for the first half of the simulation; see Fig. 7), $t_{\rm eq}/t_{\rm r1}$ initially varies approximately as $1/\mu$.

To see how this timescales manifests itself, assume for the sake of simplicity that the kinetic energy of the heavier species, E_2, dominates that of the lighter species, E_1. Equation (17) then becomes

$$\frac{dU_2}{dt} = \frac{-E_2}{t_{\rm eq}} . \tag{20}$$

Application of the usual virial theorem yields $U_2 = -E_2 = \frac{1}{2}W_2$, where W_2 is the potential energy of species 2, and so we have

$$W_2 \propto e^{t/t_{\rm eq}} . \tag{21}$$

Under the assumption that the potential of species 2 dominates, W_2 is proportional to $GM_2^2/r_{2\rm h}$, where $r_{2\rm h}$ represents any characteristic radius of species 2 but for concreteness has been chosen to be the half-mass radius. Thus,

$$r_{2\rm h} \propto e^{-t/t_{\rm eq}} , \tag{22}$$

which simply states that the timescale for contraction of the heavier species is given by $t_{\rm eq}$, the equipartition time. Equation (22) still holds true even when the potential of species 2 is not the dominant potential.

4.2. *Numerical Results*

For studying mass segregation of heavy tracers, we use as the unit of time the overall cluster relaxation time, t_r, given by equation (5). This time differs from $t_{\rm r1}$ (given by eq. [6]), the relaxation time of species 1 and the unit of time in equation (19), by a factor close to unity that varies slowly among sets of initial conditions. The quantity t_r also differs from the half-mass relaxation time, $t_{\rm rh}$ (given by eq. [7]), the unit of time used in the preceding sections for studying light tracers. A good rule of thumb is that $t_{\rm rh} \approx 0.1 t_r$ (Joshi, Rasio, & Portegies Zwart 2000).

To determine the mass segregation timescale—which should approximately equal $t_{\rm eq}$ from equation (22) but which we label τ_0—we look at the number of tracers in the halo, defined to be the region between the half-mass radius and the tidal radius, as a function of time and fit to it a decaying exponential. Figure 6 shows a representative determination of this timescale for a $W_0 = 3$, $\mu = 1.5$, $N_t = 1000$ model. Note that the exponential fit is only meaningful for the first few half-mass relaxation times, during which the ratio of velocity dispersions $\langle v_2^2\rangle/\langle v_1^2\rangle$ does not change appreciably. Figure 7 shows this ratio hovering at unity for

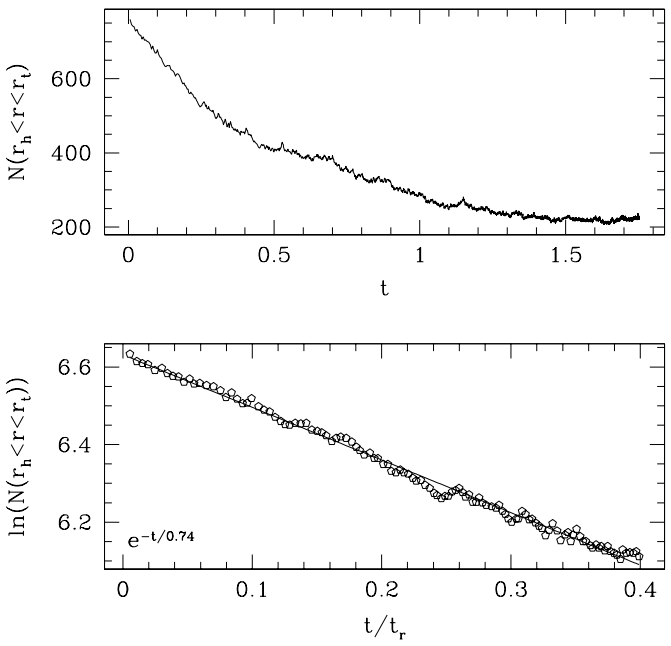

FIG. 6.—Number of tracers in the halo ($r_h < r < r_t$) as the cluster contracts, showing a representative determination of the mass segregation timescale τ_0 for the case $W_0 = 3$, $\mu = 1.5$, and $N_t = 1000$.

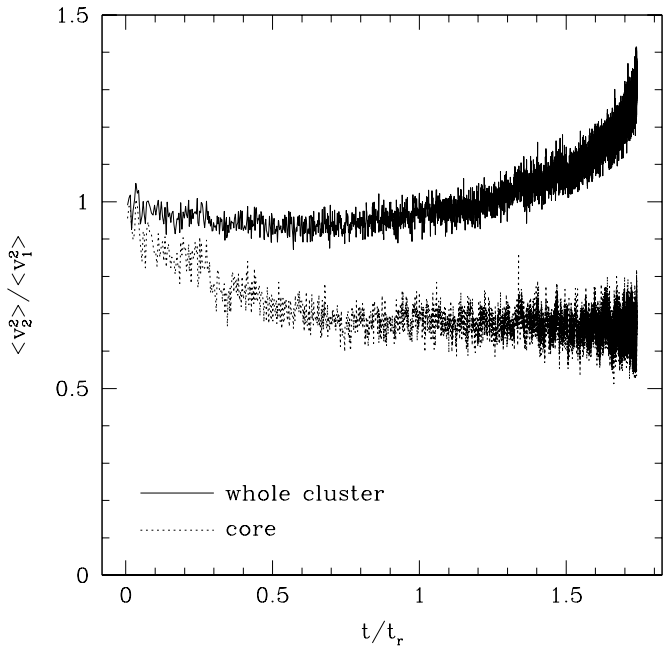

FIG. 7.—Ratio of rms velocities of the heavier component to the lighter component for the system shown in Fig. 6. Solid line is this ratio for the cluster as a whole. Note that this ratio remains near unity for about the first half of the simulation. For reference, the value of this ratio in the core is shown as a dotted line. This curve approaches 2/3, consistent with equipartition.

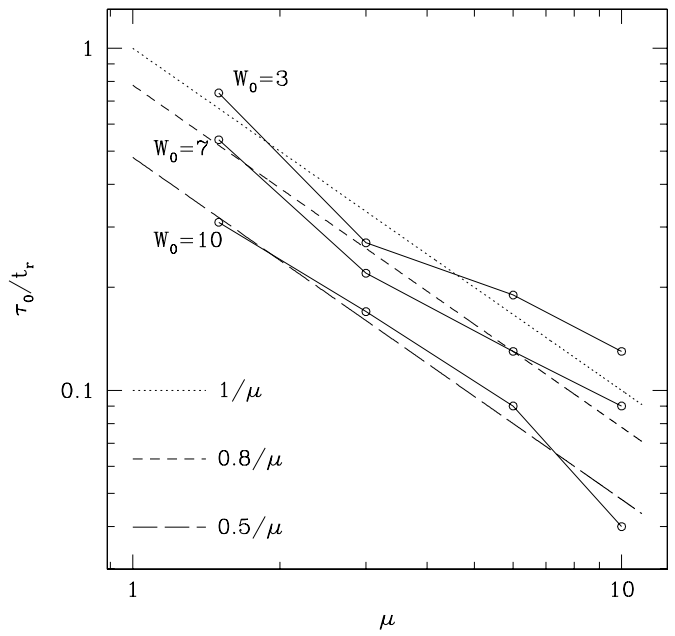

FIG. 8.—Mass segregation timescale as a function of mass ratio, for a few King initial models. In all cases $\tau_0 \propto 1/\mu$, as predicted by simple theoretical arguments.

nearly the first half of the simulation. (For reference, $\langle v_2^2 \rangle / \langle v_1^2 \rangle$ averaged over the core is shown as a dotted line. This curve approaches 2/3, consistent with thermal equilibrium.) Figure 8 shows τ_0 as a function of μ for King initial models with $W_0 = 3$, 7, and 10. In all cases, the mass segregation timescale shows a clear $1/\mu$ dependence, as expected from equation (19). Figure 9 gives another look at the segregation, showing the ratio of half-mass radii of the tracers to the background stars.

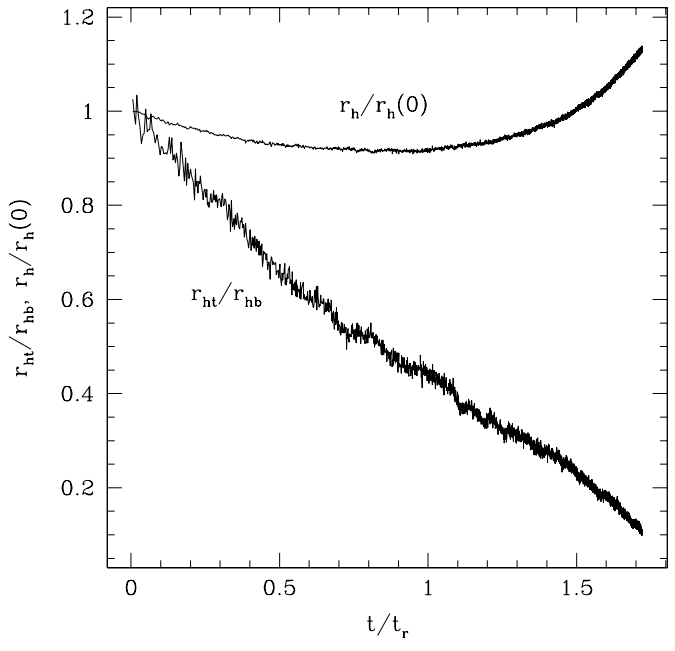

FIG. 9.—Ratio of half-mass radii of the tracers to the background stars for the system shown in Fig. 6, displaying persistent segregation. Also plotted for reference is the overall half-mass radius of the cluster.

Table 2 gives relevant initial conditions for all the heavy tracer systems considered here, as well as the thermal equilibrium stability parameters S and Λ (see eqs. [2] and [3]), core collapse times, and the ratio of half-mass radii for the two species at core collapse. Similarly to Table 1 we have included the following astrophysically relevant timescales: $\tau_0(r_h < r < r_t)$, the e-folding timescale shown in Figure 8; $\tau_{1.5}(r_c)$, the time for the number of heavy stars within the initial core radius to increase by a factor of 1.5; $\tau_{10}(r_c)$, the time for the number of heavy stars within the initial core radius to increase by a factor of 10; and $\tau_{1.5}(r_h)$, the time for the number of heavy stars within the initial half-mass radius to increase by 1.5. Here again, the trend is clear: the closer the mass ratio is to unity, the longer it takes the heavy tracers to sink into the core.

The shorter core collapse timescales for the models with larger μ or larger W_0 give these clusters little time to evolve dynamically. Consequently, mass segregation is not as pronounced in these clusters, as is evident from Table 2.

5. SUMMARY AND DISCUSSION

We have studied the mass segregation of both light and heavy tracers in two-component star clusters. The calculations were performed using our recently developed Monte Carlo code using $N = 10^5$ stars, with a few key calculations repeated using a direct N-body code running on GRAPE computers. The two methods showed good agreement in all cases. The large N that can be used in Monte Carlo simulations is essential for this type of study, as it allows us to treat a small tracer population of objects without suffering large numerical noise.

We found that light tracers with $\mu \lesssim 0.1$–0.4 (depending on cluster parameters) are ejected from the cluster core, on average, within one central relaxation time ($\sim 10^7$–10^9 yr for most globular clusters). The cores of globular clusters should therefore be largely devoid of stars of mass $\lesssim 0.25$ $M_\odot$. As a result, we predict that any observed low-mass star in a dense globular cluster core is most probably part of a binary system with a more massive companion. For example, low-mass helium white dwarfs observed in a cluster core are most probably in binary systems (Taylor et al. 2001).

Some of the low-mass objects, when they are ejected from the central region of the cluster, settle in the outer halo, where the relaxation time is so long that they are prevented from further segregation or evaporation through the tidal boundary. We found in our simulations that the number density of light tracers in the outer parts of the cluster can actually become significantly higher than it was initially. We studied the implications of these results for gravitational microlensing in globular clusters and found that low-mass objects in the cluster halo can dominate the optical depth for microlensing by up to an order of magnitude. We applied these results to the recent null detection of Sahu, Anderson, & King (2002) to estimate an upper limit on the current mass fraction of M22 in very low mass objects of $\sim$25% at the 63% confidence level.

For clusters with heavy tracers ($\mu > 1$) we found good agreement between our Monte Carlo results and direct N-body integrations, as well as simple theoretical estimates. In particular, we found that the timescale for mass segregation, τ_0, varies as $1/\mu$, as expected from theoretical predictions. Specifically, over a wide range of initial cluster concentra-

tions and mass ratios, $\tau_0/t_r = C/\mu$, where the constant $C \simeq 0.5 - 1$.

We are grateful to Eric Pfahl and Saul Rappaport for helpful discussions and comments. S. P. Z. is grateful to Northwestern University for their hospitality. This work was supported by NSF grant AST-9618116 and NASA ATP grant NAG5-8460. S. P. Z. was supported by Hubble Fellowship grant HF-01112.01-98A, awarded by the Space Telescope Science Institute, which is operated by the Association of Universities for Research in Astronomy, Inc., for NASA under contract NAS5-26555. Our Monte Carlo simulations were performed on the Cray/SGI Origin2000 supercomputer at Boston University under NCSA grant AST97-0022N. The direct *N*-body simulations were performed on the GRAPE systems at the University of Tokyo and at Drexel University.

REFERENCES

Bailyn, C. D. 1995, ARA&A, 33, 133
Bedin, L. R., Anderson, J., King, I. R., & Piotto, G. 2001, ApJ, 560, L75
Binney, J., & Tremaine, S. 1987, Galactic Dynamics (Princeton: Princeton Univ. Press)
Côté, P., Richer, H. B., & Fahlman, G. G. 1991, AJ, 102, 1358
D'Amico, N., Lyne, A. G., Manchester, R. N., Possenti, A., & Camilo, F. 2001, ApJ, 548, L171
Davies, M. B., & Sigurdsson, S. 2001, MNRAS, 324, 612
de la Fuente Marcos, R. 1996, A&A, 308, 141
Figer, D. F., et al. 1999, ApJ, 525, 750
Ford, E. B., Joshi, K. J., Rasio, F. A., & Zbarsky, B. 2000, ApJ, 528, 336
Freire, P. C., Camilo, F., Lorimer, D. R., Lyne, A. G., Manchester, R. N., & D'Amico, N. 2001, MNRAS, 326, 901
Giersz, M., & Heggie, D. C. 1997, MNRAS, 286, 709
Gilliland, R. L., et al. 2000, ApJ, 545, L47
Harris, W. E. 1996, AJ, 112, 1487
Heggie, D. C., Giersz, M., Spurzem, R., & Takahashi, K. 1998, in Highlights of Astronomy, Vol. 11, ed. J. Andersen (Dordrecht: Kluwer), 591
Heggie, D. C., Griest, K., & Hut, P. 1993, in ASP Conf. Series 50, Structure and Dynamics of Globular Clusters, ed. S. G. Djorgovski & G. Meylan (San Francisco: ASP), 137
Heggie, D. C., & Hut, P. 1996, in IAU Symp. 174, Dynamical Evolution of Star Clusters, ed. P. Hut & J. Makino (Dordrecht: Kluwer), 303
Hénon, M. 1971, Ap&SS, 14, 151
Howell, J. H., Guhathakurta, P., & Tan, A. 2000, AJ, 119, 1259
Howell, J. H., et al. 2001, AAS Meeting, 198, 9505
Jetzer, P., Strässle, M., & Wandeler, U. 1998, A&A, 336, 411
Joshi, K. J., Nave, C., & Rasio, F. A. 2001, ApJ, 550, 691
Joshi, K. J., Rasio, F. A., & Portegies Zwart, S. 2000, ApJ, 540, 969
Kroupa, P., Tout, C. A., & Gilmore, G. 1993, MNRAS, 262, 545
Layden, A. C., Ritter, L. A., Welch, D. L., & Webb, T. M. A. 1999, AJ, 117, 1313
Makino, J. 1991, ApJ, 369, 200
Makino, J., & Aarseth, S. J. 1992, PASJ, 44, 141
Makino, J., Taiji, M., Ebisuzaki, T., & Sugimoto, D. 1997, ApJ, 480, 432
Mandushev, G., Spassova, N., & Staneva, A. 1991, A&A, 252, 94
Marconi, G., et al. 1998, MNRAS, 293, 479
McMillan, S. L. W. 1986a, ApJ, 306, 552
———. 1986b, ApJ, 307, 126
Paczyński, B. 1986, ApJ, 304, 1
———. 1991, ApJ, 371, L63
———. 1994, Acta Astron., 44, 235
Portegies Zwart, S., Makino, J., McMillan, S. L. W., & Hut, P. 2002, ApJ, 565, 265
Portegies Zwart, S. F., & McMillan, S. L. W. 2000, ApJ, 528, L17
Portegies Zwart, S. F., McMillan, S. L. W., Hut, P., & Makino, J. 2001, MNRAS, 321, 199
Rasio, F. A. 2000, in ASP Conf. Ser. 202, Pulsar Astronomy: 2000 and Beyond, ed. M. Kramer, N. Wex, & R. Wielebinski (San Francisco: ASP), 589
Rasio, F. A., Fregeau, J. M., & Joshi, K. J. 2001, in The Influence of Binaries on Stellar Population Studies, ed. D. Vanbeveren (Dordrecht: Kluwer), 387
Refsdal, S. 1964, MNRAS, 128, 307
Sahu, K. C., Anderson, J., & King, I. R. 2002, ApJ, 565, L21
Sahu, K. C., Casertano, S., Livio, M., Gilliland, R. L., Panagia, N., Albrow, M. D., & Potter, M. 2001, Nature, 411, 1022
Sosin, C. 1997, AJ, 114, 1517
Spitzer, L., Jr. 1940, MNRAS, 100, 396
———. 1962, Physics of Fully Ionized Gases (2d ed.; New York: Interscience)
———. 1969, ApJ, 158, L139
———. 1987, Dynamical Evolution of Globular Clusters (Princeton: Princeton Univ. Press)
Taillet, R., Longaretti, P.-Y., & Salati, P. 1995, Astropart. Phys., 4, 87
Taillet, R., Salati, P., & Longaretti, P. 1996, ApJ, 461, 104
Takahashi, K., & Portegies Zwart, S. F. 2000, ApJ, 535, 759
Taylor, J. M., Grindlay, J. E., Edmonds, P. D., & Cool, A. M. 2001, ApJ, 553, L169
Vesperini, E., & Heggie, D. C. 1997, MNRAS, 289, 898
Vietri, M., & Ostriker, J. P. 1983, ApJ, 267, 488
Watters, W. A., Joshi, K. J., & Rasio, F. A. 2000, ApJ, 539, 331